

# Interpretation for Ground Penetrating Radar Data Based On Combination between the Wavelet Transform and the Optimal Algorithm

Tin Duong Quoc Chanh<sup>1\*</sup>, Dau Duong Hieu<sup>1</sup>, Huong Vo Thu<sup>2</sup>

<sup>1</sup> Can Tho University, Campus 2, 3/2, Ninh Kieu, Can Tho

<sup>2</sup> Vinh Thanh high school, Vinh Thanh district, Can Tho city

Corresponding Author: Tin Duong Quoc Chanh

**ABSTRACT:** In recent years, technique of ground penetrating radar (GPR) has been effectively applied among the complex of geophysics methods in geo-engineering research. In the interpretation process, crucial parameters including depth, position, and size of the buried objects are needed to determine. In this paper, the continuous wavelet transform (CWT) with the appropriate wavelet functions are introduced to determine the position and size of the buried objects by the wavelet transform modulus maxima (WTMM)-method, for enhancing the interpretation efficiency of the GPR data. In addition, Kirchhoff migration method is optimized by the minimum entropy and the maximum energy standards, allowing to determine the electromagnetic wave velocity in the material. Then, the depth from the ground to the top of the buried object is also estimated. The proposed method correctness is tested on the modeling data, and then application for analyzing the GPR data in some places of Can Tho city.

**KEYWORDS:** Ground penetrating radar (GPR), electromagnetic wave velocity, the minimum entropy and the maximum energy standards, wavelet transform modulus maxima (WTMM).

Date of Submission: 17-01-2023

Date of acceptance: 02-02-2023

## I. INTRODUCTION

In recent years, ground penetrating radar (GPR) has become a useful device in identifying underground structures with many advantages such as: no digging, no destruction, fast data collection speed, high resolution and accuracy<sup>1</sup>. It is widely applied in the study of shallow strata structure: prediction of subsidence, landslides, drawing of urban underground works, traffic, construction, archeology and many other technical fields<sup>2</sup>. Therefore, the GPR data processing methods are always improved and constantly evolving.

In the process of processing GPR data, the accurate determination of the electromagnetic wave propagation speed in the survey environment allows to obtain the best shifting cross-section, reflecting the fullest necessary information of environment below the ground to be surveyed. In fact, determining this speed is a very difficult problem because when the speed changes at close values, the cross sections obtained after the displacement often have a fairly similar form. Therefore, the selection of cross-sectional images after displacement is quite complicated and requires an optimal standard.

The migration algorithm has been used widely in GPR data processing in recent years. In 2011, the Kirchhoff migration algorithm was used to determine the propagation velocity model for GPR<sup>3</sup>. In 2013, finite differential migration<sup>4</sup> was applied to processing GPR data. The research results have helped to determine the depth and size of water supply pipes and underground cables getting small errors. In 2014, the minimum entropy technique in image processing was used in combination with migration method to determine the optimal wave transmission velocity<sup>5</sup>, initially solving the problem of quantitative processing of GPR data.

The wavelet transformation is a useful mathematical tool in analyzing of non-stop signals such as radar or GPR<sup>6</sup> data. Recently, Ouadfeul and colleagues<sup>7</sup> used WTMM method in 2-D wavelet transform to analyze magnetic, gravity and GPR data with many positive results.

In the paper, a new technique for processing GPR data is based on a combination of wavelet transformation and the optimal algorithm which was studied, applied to determine the location, size and depth of the buried pipe in the ground.

## II. DATA AND METHODS

### 2.1 Ground penetrating radar

The use of reflected electromagnetic waves to probe subsurface objects was first proposed by Cook JC in 1960<sup>8</sup>. Later, Cook and other research groups (Moffatt and Puskar, 1976)<sup>9</sup> continued their research and develop electromagnetic transceiver systems to detect relatively small objects that were reflected electromagnetic waves below the surface of the earth. The basic principle of ground-penetrating radar was detailed by Benson in 1995<sup>10</sup>. The principle can be summarized briefly, with some main points: GPR uses an antenna that transmits electromagnetic waves in the form of pulses, typically in the frequency range from 10 MHz to 3000 MHz, propagating in subsurface matter at velocities depending on the structure of the environment. When the electromagnetic wave moves, if it encounters foreign bodies or boundary surfaces with inhomogeneity in electrical properties with the surrounding environment, part of the wave energy will be reflected back to the ground or scattered into the surrounding environment. The rest of the energy continues to move inwards and repeats the above reflection and scattering process until the energy is absorbed by the environment. The reflected waves are recorded by the receiving antenna and stored in the device's memory for later processing and analysis. The reflected wave recording channels along a measuring line are arranged vertically, and they are viewed as a two-dimensional reflector cross section in the vertical direction of the stratigraphy or characteristics below the surface. When the foreign object is in front of or behind the antenna of the ground penetrating radar machine, it takes a long time for electromagnetic waves to reflect back into the antenna; meanwhile, if the antenna sweeps across the foreign object, the time the reflected waves return to the receiver will be much shorter. This phenomenon produces images of the reflected waves captured by the antenna in the form of a hyperbola. This hyperbola is the actual image of a small object (like a pipe) located at the center of the curve (Fig. 1a, 3a).

### 2.2 Continuous wavelet transform and wavelet function Farshad-Sailhac

The 1-D continuous wavelet transform is that turns a spatially 1-D signal into a 2-D function in convolution:

$$W(a,b) = \int_{-\infty}^{+\infty} f(x)\psi_{a,b}(x)dx = \langle f(x) | \psi_{a,b}(x) \rangle \quad (1)$$

Where,  $\psi_{a,b}(x)$  is the child wavelet of the mother wavelet  $\psi(x)$  at scale  $a$  and shifted  $b$ , with:

$$\psi_{a,b}(x) = \frac{1}{\sqrt{a}} \psi\left(\frac{x-b}{a}\right) \quad (2)$$

$W(a,b)$ : continuous wavelet transform coefficient of  $f(x)$ ;  $a \in R^+$ : scale parameters (inverse of frequency) that characterizes the expansion ( $a > 1$ ) or compression ( $a < 1$ ) wavelet;  $b$ : shift parameter, which provides information about the position of the translated wavelet window;  $\frac{1}{\sqrt{a}}$ : normalization coefficient.

The 2-D continuous wavelet transform (2-D CWT) is given by the expression:

$$W(a,b_x,b_y) = \frac{1}{a} \int_{-\infty}^{+\infty} \int_{-\infty}^{+\infty} f(x,y) \psi\left(\frac{x-b_x}{a}, \frac{y-b_y}{a}\right) dx dy \quad (3)$$

Where,  $\psi\left(\frac{x-b_x}{a}, \frac{y-b_y}{a}\right)$  is the child wavelet of the 2-D mother wavelet  $\psi(x,y)$ ;  $b_x, b_y$  is the shift parameter in the  $x$  and  $y$  directions.

If:  $\psi(x,y) = \psi(x)\psi(y)$ , the expression (3) can be transformed into:

$$W(a,b_x,b_y) = \int_{-\infty}^{+\infty} \int_{-\infty}^{+\infty} f(x,y) \frac{1}{\sqrt{a}} \psi\left(\frac{x-b_x}{a}\right) dx \cdot \frac{1}{\sqrt{a}} \psi\left(\frac{y-b_y}{a}\right) dy \quad (4)$$

The expression (4) will be satisfied when applying the continuous 1-D wavelet transform on two separate  $x, y$  directions<sup>11</sup>.

In the paper, the complex wavelet function Farshad-Sailhac<sup>12</sup> is given by the following expression:

$$\psi^{(FS)}(x) = \frac{4-2x^2}{(x^2+4)^{\frac{5}{2}}} - \frac{1-2x^2}{(x^2+1)^{\frac{5}{2}}} + i \cdot \left(\frac{5}{2}x - \frac{4}{5}x^3\right) \left[ \frac{1}{(x^2+4)^{\frac{5}{2}}} - \frac{1}{(x^2+1)^{\frac{5}{2}}} \right] \quad (5)$$

The Farshad-Sailhac complex wavelet will be used in the wavelet transform modulus maxima method to determine the position, and the horizontal size of the buried object.

### 2.3 The Wavelet Transform Modulus Maxima (WTMM) method

In image processing, boundary identification is a very important step. According to image processing theory, the edges of an image are the areas at which the brightness intensity has a sudden change or the color has a strong contrast. With spatially variable signals such as gravity data, or geomagnetic data, or seismic wave data, GPR, etc., the points where the amplitude of the signal changes rapidly or suddenly are considered as the boundary of the signal.

The boundary determination method uses wavelet transform based on finding the position on the scalogram at the wavelet transform coefficient is maximal. Thus, the boundary determination technique by wavelet transform<sup>13</sup> is also known as the wavelet transform modulus maxima (WTMM) method. Applying this method, GPR data analysis helps to determine the location, and size of buried objects.

### 2.4 Kirchhoff migration

This method is implemented based on Huygens – Fresnel principle and Kirchhoff problem<sup>14, 15, 16</sup>.

Electromagnetic waves when traveling into the medium, if they encounter a difference in electromagnetic properties, they will reflect back. Each point on the reflecting boundary is considered a secondary source of broadcasting, producing signal pulses in the form of a half-circle in the x-z plane or hyperbolic form in the x-t plane and transmitted to the receiver on the ground<sup>17</sup>.

### 2.5 Minimum entropy technique

In statistical physics, entropy is considered to be the quantity that measures the "chaotic" ability of a system to correspond to a certain macro state. In information theory, entropy is used to measure the amount of uncertainty (or randomness) of an event or a given random distribution. In genetic engineering, entropy is the degree of genetic freedom. In image processing, entropy refers to the disorder of pixels<sup>18, 19, 20</sup>. The large entropy values correspond to the high level of chaos. Assume that the image X of size M x N takes discrete values 1, 2, 3... with respective probabilities p<sub>1</sub>, p<sub>2</sub>, p<sub>3</sub>. ...Then the entropy is given by<sup>21, 22</sup>.

$$E(X) = -\sum_i p_i \log p_i \quad (6)$$

Using expression (6) to calculate the entropy has two computational problems, first, it is time-consuming to compute the p<sub>i</sub>, for a large image, second, if the discrete values of X are predetermined, then there is possibility that p<sub>i</sub> = 0 for some i and log0 cannot be computed. To circumvent the above problems, we use an approximation to the entropy, namely, the varimax norm. The varimax norm of an image is defined as<sup>23</sup>:

$$E(X) = -\sum_{i=1}^N \left\{ \frac{\sum_{j=1}^M X_{ij}^4}{\left[ \sum_{j=1}^M X_{ij}^2 \right]^2} \right\} \quad (7)$$

The maximum value of entropy is equal to 1.0 for the write path with only one signal pulse, whose value of N for the set N of the write line. The greater the entropy is, the greater the chaos (noise) in the image. In contrast, the entropy minimum of the image after teleportation processing can increase the convergence to its optimum level, so the shift processing efficiency will be higher when they are combined with the minimum entropy technique.

### 2.6 Maximum energy standard

According to Yilmaz et al., the migration step will help to converge the signal and filter out the noise<sup>14</sup>. So, the GPR cross section after the transition that responds to the maximum energy will have the highest reliability. At that time, the calculation speed will be closest to the real speed. However, the signal energy on the GPR cross-section depends on the existence of disturbances in the survey area. Therefore, in order to improve the image quality and increase the accuracy of the energy calculation, it is necessary to perform noise filtering steps on the GPR cross-section before shifting. After the type of interference by different methods in the processing chain, the signal energy is recorded by the system<sup>24</sup>:

$$D(j) = \sum_{i=1}^M X^2(i, j) \quad j = 1, 2, 3, \dots, N \quad (8)$$

Calculating the energy as above will take a long time and cause errors in the results, so it is necessary to select the signal region of interest Y to limit noise and eliminate unnecessary areas. From here, the process of calculating the signal energy is carried out quickly, making the processing more accurate. The process of selecting the area of interest is carried out as follows<sup>25</sup>:

From the X collection cross section, select the region of interest containing the hyperbolic signal. From here, determine the number of sample steps of the region of interest, then represent them as a Y cross section. Similar to the X cross section, the Y ( $Y \subseteq X$ ) area of interest is represented in two-dimensional arrays of K x Q size ( $K < M$ ,  $Q < N$ ).

The signal energy of the Y region is determined by system:

$$D_Y(j) = \sum_{i=1}^K Y^2(i, j) \quad j = 1, 2, 3, \dots, Q \quad (9)$$

Similar to entropy, for each velocity parameter, the section after displacement will have a certain energy value. By comparison, it is possible to determine the maximum energy value and the corresponding position of the object on the displayed image. From there, infer the corresponding velocity value.

## 2.7 The process for GPR data analysis using the wavelet transform and optimal algorithm

The processing of GPR data using a combination of wavelet transformation and optimal algorithm can be summarized in the process of the following steps:

**Step 1:** Determining the position of the buried pipe.

After processing the raw data, we are going to obtain a GPR section quite clear and complete.

Performing 2-D CWT for GPR section using Farshad-Sailhac wavelet function.

Plotting the module contours of 2-D CWT coefficients with appropriate scale ( $a$ ). The maximum point of the wavelet transform coefficients will be found. The horizontal and vertical coordinate of this point will be  $bx$  and  $bt$  respectively. The position of the buried pipe in the horizontal direction and the time for the radar waves to bounce back to the antenna will be detected by following equations:

$$x = bx \times \Delta x \quad (10)$$

$$t = bt \times \Delta t \quad (11)$$

**Step 2:** Determining the size of the buried pipe.

From the GPR section, an optimal data cutting layer (corresponding with  $bt$  in step 1) is chosen to analyze by the wavelet method.

Performing Farshad-Sailhac CWT with GPR data is selected.

Changing the different scales ( $a$ ) and repeating the multiscale CWT.

Plotting the phase contours of the CWT coefficients with different scales ( $a$ ).

The left and right edge coordination of the buried object will be found on the plot of wavelet phase contours and the size of the buried pipe will be estimated by:

$$D_x \approx [bx(p) - bx(t)] \times \Delta x = D \quad (12)$$

**Step 3:** Determining the depth of the buried pipe.

Using Kirchhoff migration method is combined with the minimum entropy and the maximum energy standards, to determine the electromagnetic wave velocity ( $v$ ) in the material.

The depth of the buried pipe will be detected by following equation:

$$z = v \times \frac{t}{2} \quad (13)$$

**Step 4:** Drawing the GPR cross-section – appropriate representation of the real environment.

Perform a Kirchhoff migration with a defined wave transfer rate ( $v$ ) from the minimum entropy standard and maximum energy to create a GPR cross section – reflecting the real environment.

## III. RESULTS AND DISCUSSION

### 3.1 Theoretical model

To test the reliability of the proposed method, various theoretical models conducted tests including: buried objects are cylindrical tubes as well as square tubes, made from different materials such as plastic, metal, concrete. These buried objects are also designed in many different sizes. They are very close to the supply and drainage pipes, telecommunication cable protection pipes, power cables, technical boxes... as a reality and they are buried in environments that are not the same from simple to complex. The relative deviation obtained from the results of the analysis of the model data is acceptable and within the limits that allow to prove that the analytical method is reliable. In this paper, the results of processing on the typical theoretical model will be introduced to illustrate the analytical method.

In this model, using an antenna (in GPR machine) with a frequency of 700 MHz, the heterogeneous environment consists of three horizontal layers:

The first layer, asphalt has thickness 0.2 m, conductivity  $\sigma = 0.001$  mS/m, relative dielectric constant  $\epsilon_r = 4.0$ , constant from relative lips  $\mu_r = 1.0$ , electromagnetic wave propagation speed  $v_1 = 0.15$  m/ns.

The second layer, breakstone has thickness 0.4 m,  $\sigma = 1.0$  mS/m,  $\epsilon_r = 10.0$ ,  $\mu_r = 1.0$ ,  $v_2 = 0.10$  m/ns.

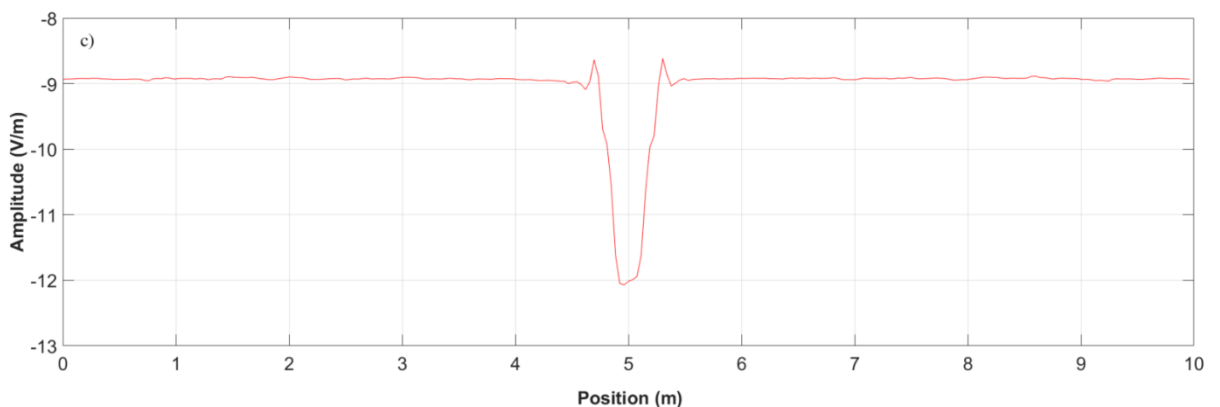
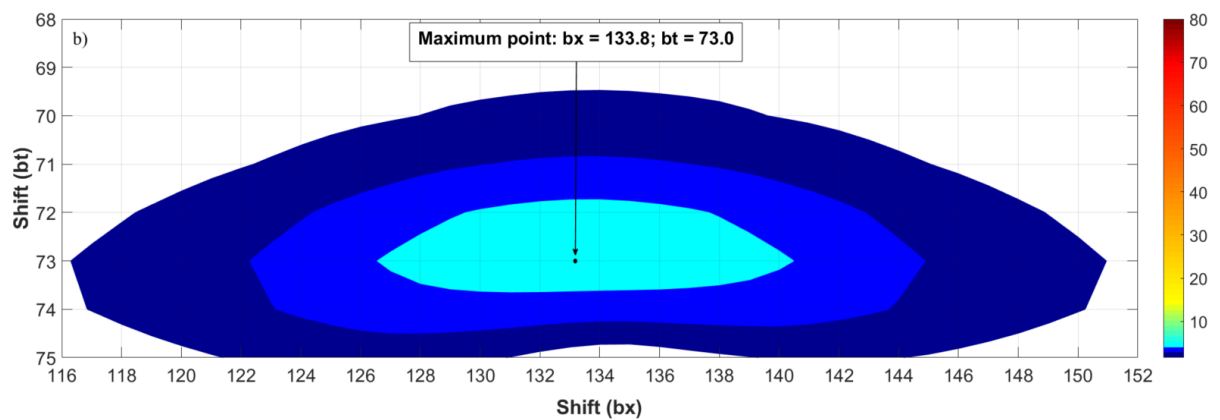
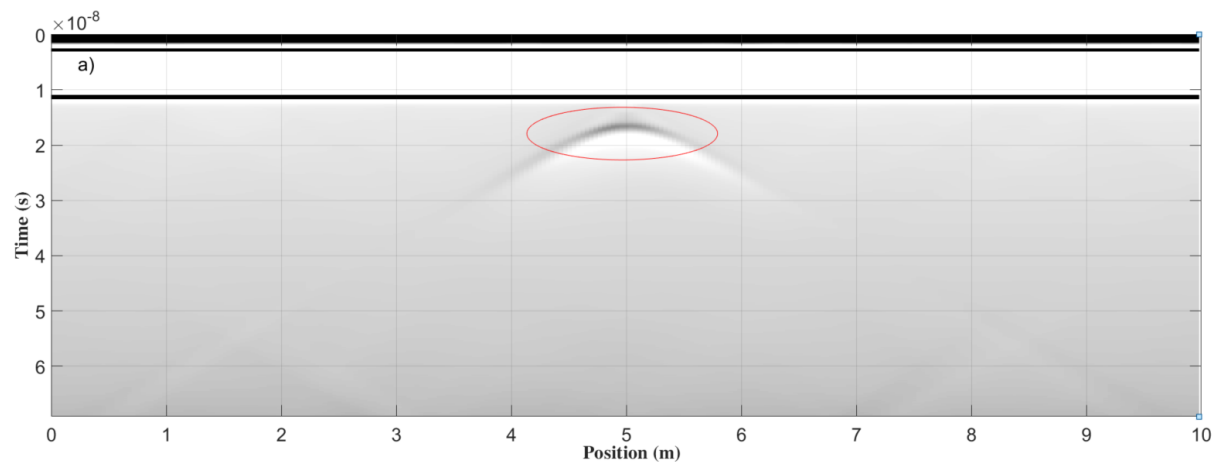
The final one, clay soil has thickness 4.4 m,  $\sigma = 200$  mS/m,  $\epsilon_r = 16.0$ ,  $\mu_r = 1.0$ ,  $v_s = 0.07$  m/ns.

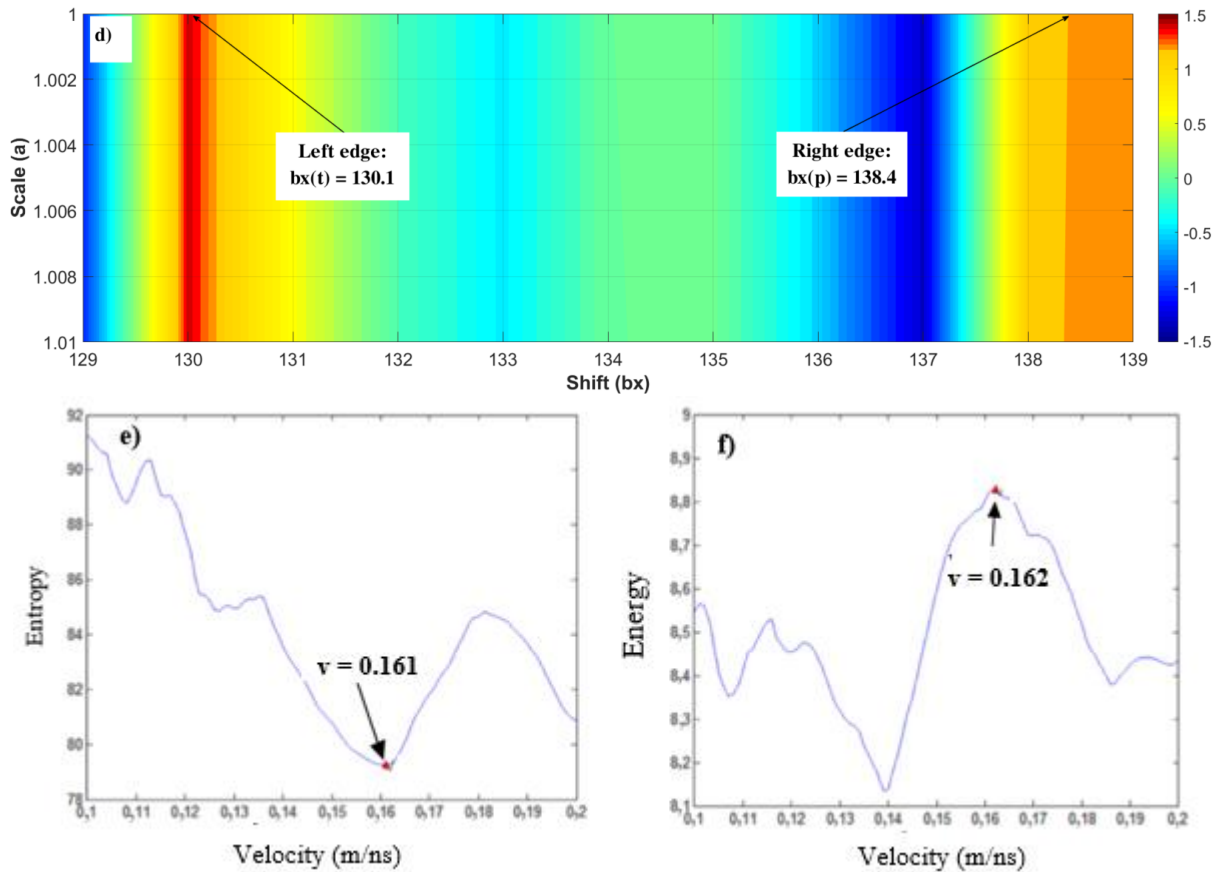
Underneath anomaly object is a concrete cylinder:  $\sigma = 1.0$  mS/m;  $\epsilon_r = 6.0$ ;  $\mu_r = 1.0$ ;  $v' = 0.12$  (m/ns), inside contains the air, the center of the object is located at horizontal coordination  $x = 5.00$  m; and vertical coordination  $z = 0.80$  m; inside pipe diameter  $d = 0.30$  m; outside pipe diameter  $D = 0.32$  m. The 10.0 m long ground measurement line cuts across the foreign object, the measuring step is  $\Delta x = 0.03788$  m.

Figure 1a shows the GPR cross-section of the model, there exists a forward-biased hyperbola at position  $x = 5.0$  m and  $t = 10.5$  ns, which proves the signal is reflected from the concrete pipe (conductivity less than the medium).

The result of drawing the 2-D wavelet transform coefficient at the scale  $a = 10$  shown in Figure 1b allows to determine the maximum point coordinates ( $bx = 133.8$ ;  $bt = 73.0$ ).

The reflected wave amplitude signal along the  $bt = 73.0$  is extracted from the GPR cross section (Fig. 1c) to perform the wavelet transformation. The results of the phase contour drawing shown in Fig. 1d allow to determine the coordinates of the left and right margins of the buried object, respectively:  $bx(t) = 130.1$ ;  $bx(p) = 138.4$ . Therefore, the size of the object can be estimated from the expression (12).





**Fig. 1.** The graphs of the theoretical model. a) GPR section of the model, b) The signal of the row beneath hyperbolic peak, c) The module contour of 2-D CWT, d) The phase contour of the wavelet transform, e) The relation between entropy and velocity, f) The relation between energy and velocity

The results of calculation of entropy and energy by speed are shown in Fig. 1e, 1f, respectively, allowing to determine the speed of electromagnetic wave propagation in the medium as 0.161 (m/ns) - corresponding to minimum entropy or 0.162 (m/ns) - corresponds to the maximum energy. From there, the depth to the top of the foreign body can be estimated according to formula (13).

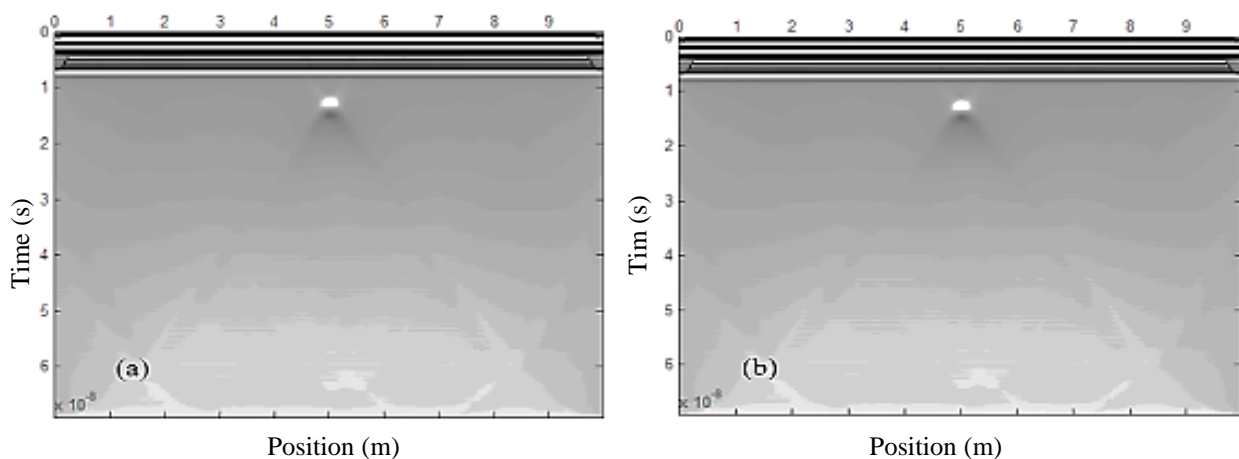


**Fig. 2.** GPR cross section after migration. a) velocity  $v = 0.161$  m/ns, b) velocity  $v = 0.162$  m/ns

The results of the model analysis are presented in detail as shown in Table 1.

**Table 1:** Model analysis results

Model parameters		Relative errors
Position	$x = 5.0\text{ m}$	
Size	$D = (138.4-130.1) \times 0.03788 = 0.31\text{ m}$	3.1%
Depth	$z = 0.161 \times \frac{10.5}{2} = 0.85\text{ m}$	6.3%

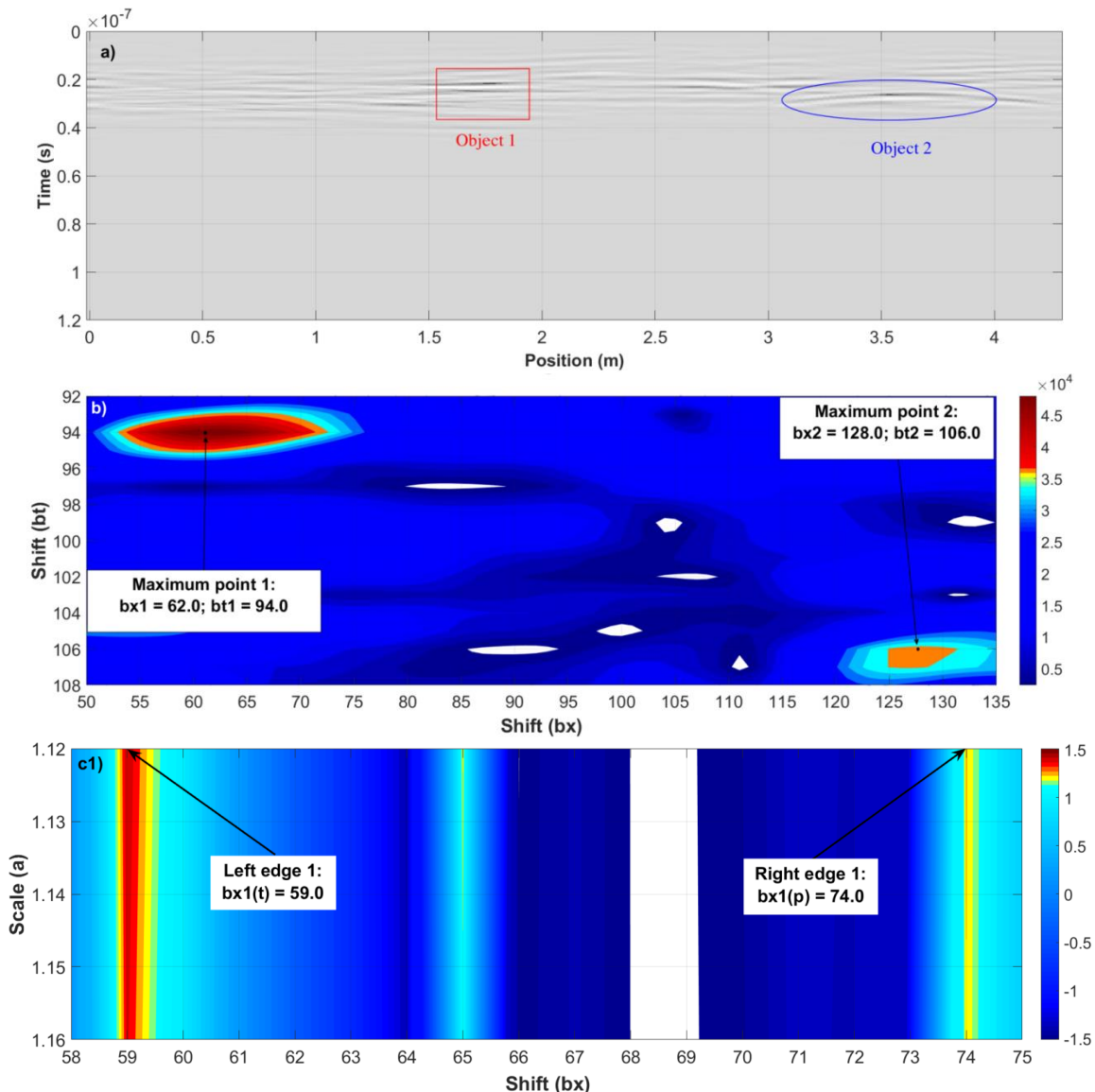
The results of the analysis presented in Table 1 indicate that the identification of the basic parameters of the buried pipe in the heterogeneous environment of the model has minor deviations (3.1% and 6.3% respectively for the determination of size and depth).

In addition, performing Kirchhoff migration at the speed of electromagnetic wave transmission (determined from the minimum entropy and maximum energy standards) allows the construction of the GPR cross section – a consistent representation of the real environment Fig. 2a, 2b.

In order to assess the applicability to the reality of the proposed method, GPR measurement data on some roads in Can Tho City has been analyzed for positive results. In this article, a typical data profile is chosen for interpretation.

**3.2 Actual data - Engineering box and drainage pipe**

GPR data was recorded by Duo detector (IDS, Italia), using antenna at frequency of 700 MHz. The profile LZZ20026 was done in front of house No. 86, Street No. 2, Staff Housing Area, Teachers of Can Tho University, Ninh Kieu District, Can Tho City. The length of the profile was 4.30 m, with the step size of  $\Delta x = 0.02784\text{ m}$ .



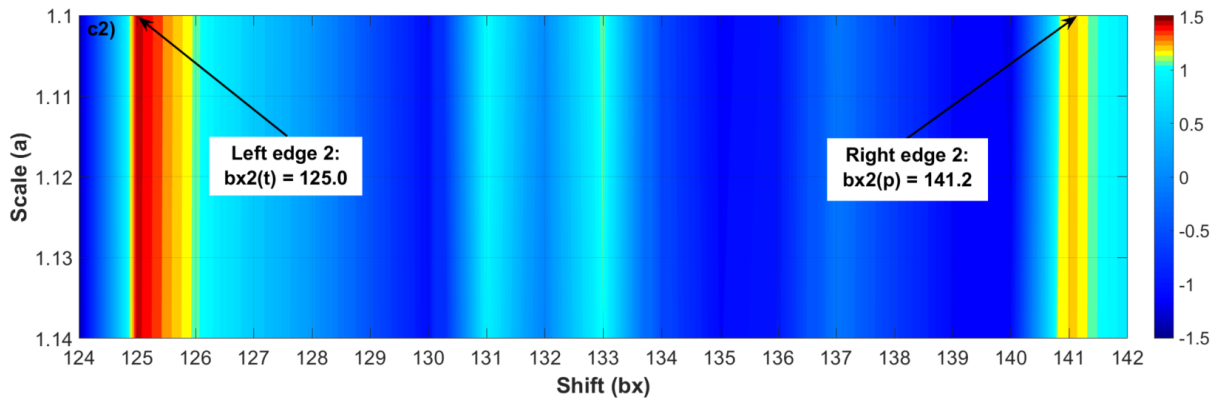


**Fig. 3.** The graphs of the actual data. a) GPR section of the engineering box and drainage pipe data, b) The module contour of 2-D CWT, c1, c2) The phase contour of the wavelet transformation on the signal along the  $bt_1 = 94.0$ ;  $bt_2 = 106.0$

Observing the GPR cross section as shown on Fig. 3a, shows that a strong reflector signal appears in a horizontal flat form in the position ( $x_1 = 1.70$  m;  $t_1 = 23.0$  ns), predicting this is a technical box with a flat cover (buried object 1) and a polarizing hyperbolic signal in place ( $x_2 = 3.65$  m;  $t_2 = 27.3$  ns) (buried object 2) should be this buried object has a lower conductivity than the surrounding environment, predicting this is a concrete drainage pipe.

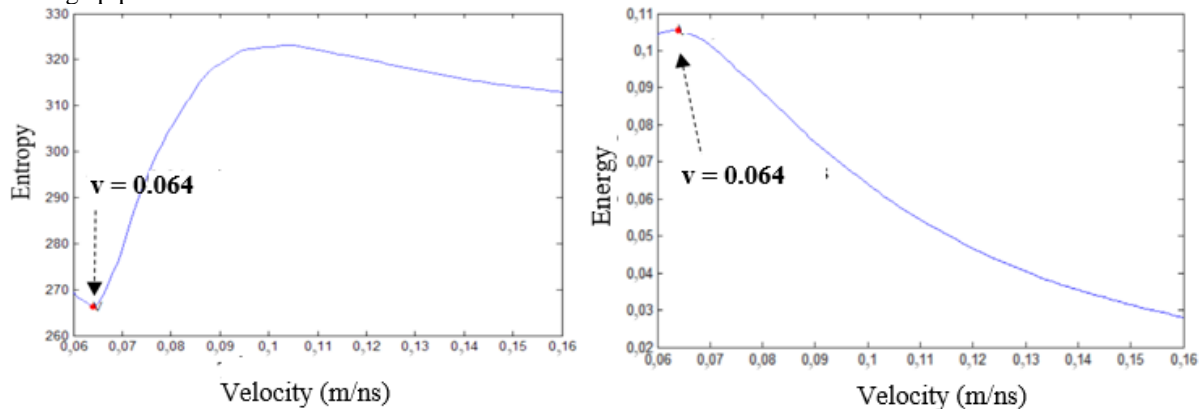


**Fig. 4.** The relation between entropy, energy and velocity (area of interest around buried object 1)

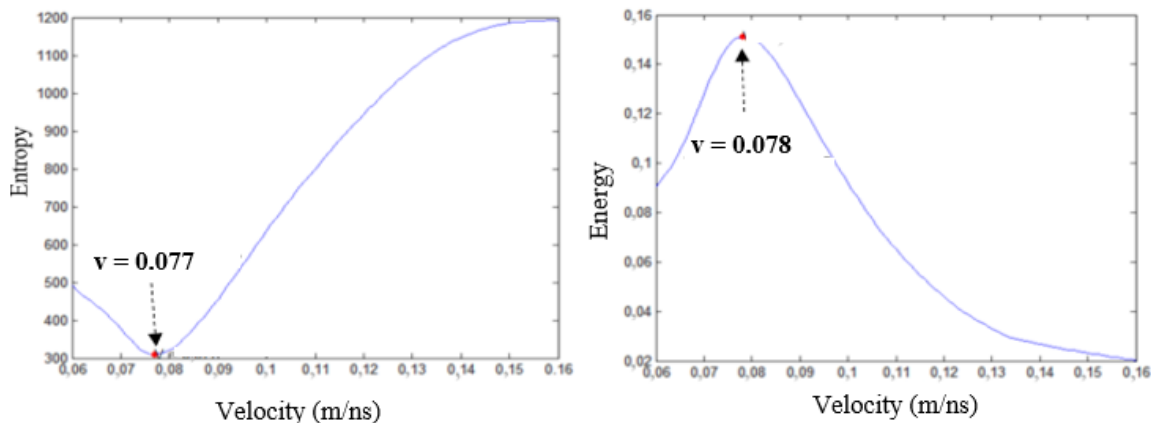


**Fig. 5.** The relation between entropy, energy and velocity (area of interest around buried object 2)

The results of the 2-D wavelet transform coefficient drawing using the Farshad-Sailhac wavelet function is shown on Fig. 3b help to determine the coordinates of two maximum points: ( $bx_1 = 62.0$ ;  $bt_1 = 94.0$ ) and ( $bx_2 = 128.0$ ;  $bt_2 = 106.0$ ).

The reflected wave signal data along the  $bt_1 = 94,0$  (passing through the top of object 1) and  $bt_2 = 106.0$  (through the top of object 2) are extracted from the GPR cross section to perform the wavelet 1-D transformation.

According to the results of the wavelet transform coefficient phase drawing shown as shown in Fig. 3c1, 3c2, the position of the left and right edges of the two buried objects are also determined as:  $bx_1(t) = 59.0$ ;

$bx_1(p) = 94.0$  and  $bx_2(t) = 125.0$ ;  $bx_2(p) = 141.2$ . Then the size of the two buried objects will be estimated from the formula (12).

Figure 4, and Figure 5 show entropy and energy calculation results with velocity. This result allows to determine the velocity of electromagnetic wave transmission in the environment above buried object 1 is 0.064 (m/ns) and above object 2 is 0.077 m/ns - corresponding to the minimum entropy or 0.078 (m/ns) - in response to the maximum energy.

From that, the depth to the top of two buried objects is determined according to the formula (13).

The results of the analysis are presented in detail as in Table 2.

According to the prior information (provided by the designer and installer), the size of this technical box and drainage pipe are  $D_1 = 0.40$  m,  $D_2 = 0.50$  m respectively. This information helps to determine the deviation between the calculated value and the actual value.

Perform Kirchhoff migration at velocity  $v = 0.064$  m/ns and  $v = 0.077$  m/ns, the resulting GPR cross section is shown specifically as Fig 6.

Observation of the shifting GPR cross section shown through Fig. 6a shows that at the position of 1.70 m, the image showing buried object 1 represents roughly the surface of the object (not a hyperbole), while the image of the buried object 2 at the coordinates of 3.65 m has a slightly curved form down indicating that the wave transmission speed above the object is greater than 0.064 m/ns.

**Table 2:** Results of analysis of GPR data of route 2, Ninh Kieu District

Actual parameters		Relative errors
Position	$x_1 = 1.70$ m	
	$x_2 = 3.65$ m	
Size	$D_1 = (74.0-59.0) \times 0.02784 = 0.42$ m	4.3%
	$D_2 = (141.2-125.0) \times 0.02784 = 0.45$ m	9.8%
Depth	$z_1 = 0.064 \times \frac{23.0}{2} = 0.74$ m	
	$z_2 = 0.077 \times \frac{27.3}{2} = 1.05$ m	

Similarly, with the shifting GPR cross section is shown in Fig 6b, the object 2 has clearly gathered, the object 1 still displays the image representing roughly the surface of the object.

In summary, GPR data analysis based on the combination of wavelet transform and optimization algorithm plays an important role in determining the location, size and depth of buried objects in shallow soil layers in heterogeneous environments. After that, the next job is to remove foreign objects from the environment or put more pipes into the ground. This will be done quite quickly, saving construction time and contributing to improving economic efficiency.

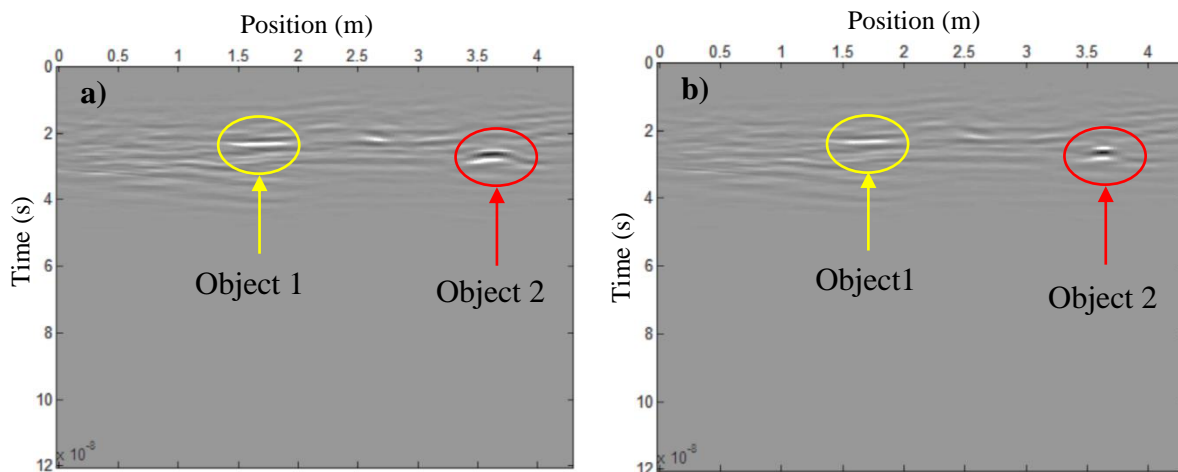


**Fig. 6.** GPR cross section after displacement. a) velocity  $v = 0.064$  m/ns, b) velocity  $v = 0.077$  m/ns

#### IV. CONCLUSION

GPR data analysis procedure based on a combination of wavelet transform and optimization algorithm has been successfully built and applied to determine the location, size and depth of buried objects, as well as draw the GPR cross-section – representing the real environment below the ground. The article illustrates the application of the process to analyze a typical theoretical model and a typical actual data measurement route. The theoretical model is designed with parameters close to the actual research objects to verify the reliability of

the method before applying it in practice. With model data, the error of determining the size and depth of buried bodies is 3.1% and 6.3%, respectively, demonstrating the high reliability of the method. With the actual measurement data, the results of determining the size of the technical box and the drainage pipe have a deviation of 4.3% and 9.8%, confirming the applicability of the method in practice. The velocity of electromagnetic wave propagation in the environment is determined from the minimum entropy standard and the maximum energy allows to determine the depth of the foreign body as well as drawing the GPR cross-section – reflecting the real environment below the ground. The results are consistent when using only wavelet transform to determine the size of buried bodies, this confirms the effectiveness of the combination of wavelet transform and optimization algorithm in interpreting GPR data.

#### ACKNOWLEDGMENT

This study is funded in part by the Can Tho University, Code: T2022-102.

#### REFERENCES

- [1]. Daniels D. J., Ground Penetrating Radar, The Institution of Electrical Engineers, UK, 2004; p. 752.
- [2]. Van N. T., and Giang N. V., Ground penetrating radar – Methods and Applications, Vietnam National University Ho Chi Minh City Press, 2013; pp. 222.
- [3]. Cuong, L.V.A., Trung, D.H., Van, N.T., Giang, N.V., and Triet N.M. Kirchhoff migration for specifying velocity model in high frequency electromagnetic method, Journal of the Earth Sciences, 2011;33(2), 142-150, Available from: <https://doi.org/10.15625/0866-7187/33/2/319>.
- [4]. Trung, D.H., Hai, Đ.T.T., Van, N.T. Using the finite difference migration method to process the GPR data, Journal of Marine Science and Technology, ISSN 1859-3097, 2013; 13(3A), 120-126.
- [5]. Van, N.T., Thuan, N.V., Trung, D.H. Frequency-wavenumber (F-K) migration and minimum entropy standard for processing GPR data, Journal of Geology, 2014; Series A (341-345), 273-282.
- [6]. Jamal B., Samer L., Mounir H., Imad L., Al-Qadi, and Kmel B., GPR signal de – noising by discrete wavelet transform, Elsevier, NDT and E. International, 2009; 42, pp. 696-703.
- [7]. Ouadfeul S., Aliouane L., Hamoudi M., Boudella A., and Eladj S., Multiscale Analysis of Geophysical Signals Using the 2-D Continuous Wavelet Transform, Wavelet Transforms and Their Recent Applications in Biology and Geoscience, Published by InTech, Croatia, 2012; pp. 253-276.
- [8]. Cook J. C., Proposed monocyte-pulse VHF radar for airborne ice and snow measurements. Journal of the American Institute of Electrical Engineers, Transactions on Communication and Electronics, 1960; 79, pp. 588-594.
- [9]. Moffatt D. L., Puskar R. J., A subsurface electromagnetic pulse radar, Geophysics, 1976; 41, pp. 506-518.
- [10]. Benson A. K., Applications of ground penetrating radar in assessing some geological hazards—examples of groundwater contamination, faults, cavities. Applied Geophysics. 1995; 33, pp. 177-193.
- [11]. Yang Y, Li Y, Liu T. Continuous wavelet transform, theoretical aspects and application to aeromagnetic data at the Huanghua Depression, Dagang Oilfield, China. Geophysical Prospecting, European Association of Geoscientists & Engineers. 2010; 58: 669-684. Available from: [doi.org/10.1111/j.1365-2478.2009.00847.x](https://doi.org/10.1111/j.1365-2478.2009.00847.x).
- [12]. Tin D Q C. Using multiscale wavelet transform to interpretation geomagnetic, gravity, GPR data. PhD Thesis, University of Science, VNU HCM City; 2019; pp. 164.
- [13]. Mallat S, Hwang W L. Singularity Detection and Processing with Wavelets. IEEE Transactions on information Theory. 1992; 38 (2): 617-43. Available from: [doi: 10.1109/18.119727](https://doi.org/10.1109/18.119727).
- [14]. Yilmaz, O. Seismic data analysis, USA, Society of Exploration Geophysicists. 2001; Available from: <https://doi/pdf/10.1190/1.9781560801580.fm>.
- [15]. Cuong, L.V.A., Trung, D.H., Van, N.T., Giang, N.V., and Triet N.M. The Kirchhoff migration: effect of aperture parameter, Journal of the Earth Sciences, 2009; 31(4), 307-310. Available from: <https://doi.org/10.15625/0866-7187/31/4/9720>.
- [16]. Vardy, M.E., and Henstock, T.J. A frequency-approximated approach to Kirchhoff migration, Geophysics, 2010; 75(6), 211-218. Available from: <https://doi.org/10.1190/1.3491196>.
- [17]. Cuong, L.V.A., Trung, D.H., Van, N.T., Giang, N.V., and Triet N.M. Kirchhoff migration for specifying velocity model in high frequency electromagnetic method, Journal of the Earth Sciences, 2011; 33(2), 142-150. Available from: <https://doi.org/10.15625/0866-7187/33/2/319>.
- [18]. Xu, X., Miller, E.L., and Rappaport, C.M. Minimum Entropy Regularization in Frequency-Wavenumber Migration to Localize Subsurface Objects, IEEE Transactions on geoscience and remote sensing, 2003; 41(8), 1804-1812.
- [19]. Flores-Tapia D., and Pistorius S. An Entropy-Based Propagation Speed Estimation Method for Near-Field Subsurface Radar Imaging, Advances in Signal Processing, 2010. Available from: <http://doi.10.1155/2010/636458>.
- [20]. Zhou, H., Wan, X., Li, W., and Jiang, Y. Combining F-K filter with minimum entropy stolt migration algorithm for subsurface object imaging and background permittivity estimation, Procedia Engineering, 2011; 23(5), 636-641. Available from: <http://doi.org/10.1016/j.proeng.2011.11.2558>.
- [21]. Benedetto, F., Tosti, F., and Alani, A.M. An Entropy-Based Analysis of GPR Data for the assessment of Railway Ballast Conditions, IEEE Transactions on Geoscience and Remote Sensing, 2017; 55(7), 3900 - 3908.
- [22]. Candra, P., Huston, D. R., Xia, T., and Wang, G. 2D Entropy and Short Time Fourier Transform for Ground Penetrating Radar Data Analysis, Proceedings of Nondestructive Characterization or Composite Materials, Aerospace engineering, Civil Infrastructure, and Homeland Security, SPIE. 2013. Available from: <https://doi.org/10.1117/12.2010224>.
- [23]. Xu, X., and Miller, E.L. Entropy Optimized Contrast Stretch to Enhance Remote Sensing Imagery, Proceedings of 16th International Conference on Pattern Recognition, 2002; 3, 915-918.
- [24]. Thuan, N.V., Cuong, L.V.A., Van, N.T., Trung, Đ.H., Triet, V.M, and Lieu, V.N.N. Energy Analysis in Semiautomatic and Automatic Velocity Estimation for Ground Penetrating Radar Data in Urban Areas: Case Study in Ho Chi Minh City, Vietnam, Advances and Applications in Geospatial Technology and Earth Resources, Springer International Publishing. 2017; pp 34-51. Available from: [https://doi.org/10.1007/978-3-319-68240-2\\_3](https://doi.org/10.1007/978-3-319-68240-2_3).
- [25]. Van, N.T., Thuan, N.V., and Trung, D.H. Combination of Kirchhoff migration method and the energy diagram in the process of ground penetrating radar data, Science and Technology Development, 2015; 18(5), 42-50.